Optical forces through guided light deflections

Darwin Palima,[1,*] Andrew Rafael Bañas,[1] Gaszton Vizsnyiczai,[2] Lóránd Kelemen,[2] Thomas Aabo,[1] Pál Ormos,[2] and Jesper Glückstad[1,3]

[1]*DTU Fotonik, Dept. of Photonics Engineering, Technical University of Denmark, DK-2800, Kgs. Lyngby, Denmark*
[2]*Institute of Biophysics, Biological Research Centre, Hungarian Academy of Sciences, Szeged H-6701, Hungary*
[3]*jesper.gluckstad@fotonik.dtu.dk*
[*]*dazp@fotonik.dtu.dk*
www.ppo.dk

Abstract: Optical trapping and manipulation typically relies on shaping focused light to control the optical force, usually on spherical objects. However, one can also shape the object to control the light deflection arising from the light-matter interaction and, hence, achieve desired optomechanical effects. In this work we look into the object shaping aspect and its potential for controlled optical manipulation. Using a simple bent waveguide as example, our numerical simulations show that the guided deflection of light efficiently converts incident light momentum into optical force with one order-of-magnitude improvement in the efficiency factor relative to a microbead, which is comparable to the improvement expected from orthogonal deflection with a perfect mirror. This improvement is illustrated in proof-of-principle experiments demonstrating the optical manipulation of two-photon polymerized waveguides. Results show that the force on the waveguide exceeds the combined forces on spherical trapping handles. Furthermore, it shows that static illumination can exert a constant force on a moving structure, unlike the position-dependent forces from harmonic potentials in conventional trapping.

OCIS codes: (170.4520) Optical confinement and manipulation; (220.4000) Microstructure fabrication; (230.7370) Waveguides.

References and links

1. K. Dholakia and T. Cizmar, "Shaping the future of manipulation," Nat. Photonics **5**(6), 335–342 (2011).
2. J. Glückstad, "Optical manipulation: Sculpting the object," Nat. Photonics **5**(1), 7–8 (2011).
3. S. Sukhov and A. Dogariu, "Negative Nonconservative Forces: Optical "Tractor Beams" for Arbitrary Objects," Phys. Rev. Lett. **107**(20), 203602 (2011).
4. J. Chen, J. Ng, Z. Lin, and C. T. Chan, "Optical pulling force," Nat. Photonics **5**(9), 531–534 (2011).
5. G. A. Swartzlander, Jr., T. J. Peterson, A. B. Artusio-Glimpse, and A. D. Raisanen, "Stable optical lift," Nat. Photonics **5**(1), 48–51 (2011).
6. N. K. Metzger, M. Mazilu, L. Kelemen, P. Ormos, and K. Dholakia, "Observation and simulation of an optically driven micromotor," J. Opt. **13**(4), 044018 (2011).
7. M. Padgett and R. Bowman, "Tweezers with a twist," Nat. Photonics **5**(6), 343–348 (2011).
8. A. Ashkin, "Acceleration and trapping of particles by radiation pressure," Phys. Rev. Lett. **24**(4), 156–159 (1970).
9. S. Maruo, O. Nakamura, and S. Kawata, "Three-dimensional microfabrication with two-photon-absorbed photopolymerization," Opt. Lett. **22**(2), 132–134 (1997).
10. B. Koss, S. Chowdhury, T. Aabo, S. K. Gupta, and W. Losert, "Indirect optical gripping with triplet traps," J. Opt. Soc. Am. B **28**(5), 982–985 (2011).
11. D. B. Phillips, J. A. Grieve, S. N. Olof, S. J. Kocher, R. Bowman, M. J. Padgett, M. J. Miles, and D. M. Carberry, "Surface imaging using holographic optical tweezers," Nanotechnology **22**(28), 285503 (2011).
12. D. Palima, A. R. Bañas, G. Vizsnyiczai, L. Kelemen, P. Ormos, and J. Glückstad, "Wave-guided optical waveguides," Opt. Express **20**(3), 2004–2014 (2012).
13. P. J. Rodrigo, L. Kelemen, D. Palima, C. A. Alonzo, P. Ormos, and J. Glückstad, "Optical microassembly platform for constructing reconfigurable microenvironments for biomedical studies," Opt. Express **17**(8), 6578–6583 (2009).

#176697 - $15.00 USD Received 21 Sep 2012; revised 22 Nov 2012; accepted 23 Nov 2012; published 7 Jan 2013

14. Y. Roichman, B. Sun, Y. Roichman, J. Amato-Grill, and D. G. Grier, "Optical forces arising from phase gradients," Phys. Rev. Lett. **100**(1), 013602 (2008).
15. M. Mahamdeh, C. P. Campos, and E. Schäffer, "Under-filling trapping objectives optimizes the use of the available laser power in optical tweezers," Opt. Express **19**(12), 11759–11768 (2011).
16. S. N. S. Reihani and L. B. Oddershede, "Optimizing immersion media refractive index improves optical trapping by compensating spherical aberrations," Opt. Lett. **32**(14), 1998–2000 (2007).
17. N. B. Simpson, D. McGloin, K. Dholakia, L. Allen, and M. J. Padgett, "Optical tweezers with increased axial trapping efficiency," J. Mod. Opt. **45**(9), 1943–1949 (1998).
18. V. Bormuth, A. Jannasch, M. Ander, C. M. van Kats, A. van Blaaderen, J. Howard, and E. Schäffer, "Optical trapping of coated microspheres," Opt. Express **16**(18), 13831–13844 (2008).
19. A. Jannasch, A. F. Demirörs, P. D. J. van Oostrum, A. van Blaaderen, and E. Schäffer, "Nanonewton optical force trap employing anti-re ection coated, high-refractive-index titania microspheres," Nat. Photonics **6**(7), 469–473 (2012).
20. S. J. Parkin, R. Vogel, M. Persson, M. Funk, V. L. Loke, T. A. Nieminen, N. R. Heckenberg, and H. Rubinsztein-Dunlop, "Highly birefringent vaterite microspheres: production, characterization and applications for optical micromanipulation," Opt. Express **17**(24), 21944–21955 (2009).
21. S. L. Neale, M. P. MacDonald, K. Dholakia, and T. F. Krauss, "All-optical control of microfluidic components using form birefringence," Nat. Mater. **4**(7), 530–533 (2005).
22. T. Asavei, V. L. Y. Loke, M. Barbieri, T. A. Nieminen, N. R. Heckenberg, and H. Rubinsztein-Dunlop, "Optical angular momentum transfer to microrotors fabricated by two-photon photopolymerization," New J. Phys. **11**(9), 093021 (2009).
23. S. Maruo, A. Takaura, and Y. Saito, "Optically driven micropump with a twin spiral microrotor," Opt. Express **17**(21), 18525–18532 (2009).
24. A. Ashkin, "Forces of a single-beam gradient laser trap on a dielectric sphere in the ray optics regime," Biophys. J. **61**(2), 569–582 (1992).
25. T. Čižmár, M. Mazilu, and K. Dholakia, "In situ wavefront correction and its application to micromanipulation," Nat. Photonics **4**(6), 388–394 (2010).
26. P. C. Ke and M. Gu, "Characterization of Trapping Force on Metallic Mie Particles," Appl. Opt. **38**(1), 160–167 (1999).
27. L. A. Ambrosio and H. E. Hernández-Figueroa, "Inversion of gradient forces for high refractive index particles in optical trapping," Opt. Express **18**(6), 5802–5808 (2010).
28. D. C. Benito, S. H. Simpson, and S. Hanna, "FDTD simulations of forces on particles during holographic assembly," Opt. Express **16**(5), 2942–2957 (2008).
29. K. S. Yee, "Numerical solution of initial boundary value problems involving Maxwell's equations in isotropic media," IEEE Trans. Antenn. Propag. **14**(3), 302–307 (1966).
30. A. Buzas, L. Kelemen, A. Mathesz, L. Oroszi, G. Vizsnyiczai, T. Vicsek, and P. Ormos, "Light sailboats: Laser driven autonomous microrobots," Appl. Phys. Lett. **101**(4), 041111 (2012).
31. L. Kelemen, S. Valkai, and P. Ormos, "Integrated optical motor," Appl. Opt. **45**(12), 2777–2780 (2006).
32. H. U. Ulriksen, J. Thøgersen, S. Keiding, I. Perch-Nielsen, J. Dam, D. Z. Palima, H. Stapelfeldt, and J. Glückstad, "Independent trapping, manipulation and characterization by an all-optical biophotonics workstation," J. Eur. Opt. Soc. Rap. Pub. **3**, 080341–080345 (2008).
33. A. La Porta and M. D. Wang, "Optical torque wrench: angular trapping, rotation, and torque detection of quartz microparticles," Phys. Rev. Lett. **92**(19), 190801 (2004).
34. S.H. Simpson, D.B. Phillips, D.M. Carberry, and S. Hanna, "Bespoke optical springs and passive force clamps from shaped dielectric particles," J. Quant. Spectrosc. Radiat. Transf. (advanced online publication 29 October 2012) *http://dx.doi.org/10.1016/j.jqsrt.2012.10.014*
35. S. H. Simpson and S. Hanna, "Thermal motion of a holographically trapped SPM-like probe," Nanotechnology **20**(39), 395710 (2009).

1. Introduction

Light can exert force and induce mechanical effects by exchanging momentum with matter. This momentum exchange depends both on the spatial distribution of the illuminating light as well as the object's refractive index distribution. Applications of optical trapping and manipulation rely upon controlling this exchange that, in general, will require both the control over the light illumination [1] as well as the object shape [2]. The widespread commercial accessibility of spatial light modulation technologies in recent years has helped channel research activities towards light-based optimization of optical forces and torques. At the same time, effects like 'optical pulling force' [3, 4], 'stable optical lift' [5], and optical micromotors [6, 7] emphasize the role of the object shape for exploiting mechanical effects from optical momentum.

#176697 - $15.00 USD Received 21 Sep 2012; revised 22 Nov 2012; accepted 23 Nov 2012; published 7 Jan 2013

Spherical beads, which have been used since Ashkin's pioneering experiments [8], have been favorite structures for optical trapping research, partly owing to their practical accessibility when performing experiments as well as the tractability of a dielectric microsphere model for theoretical analyses. However, there has been a rising prominence of three-dimensional fabrication techniques via laser direct-write methods (e.g. multiphoton polymerization [9]), with complete systems now being made available from commercial suppliers. With such systems capable of producing structures having near-arbitrary topologies and subwavelength resolutions it is, hence, worth examining structure-based approaches for the optimization of light-matter interaction. Such force-optimized structures can, e.g. replace beads in so-called "optical grippers" for indirect cell handling [10], and can also be used as optical trapping handles in optically-steered microtools [11, 12] and optical micro-assembly [13]. Optimized structures can serve to enhance optical forces in standard optical tweezer systems, as well as possibly enable strong optical trapping using only moderate to low numerical aperture lenses, which can avoid intensity hotspots and provide a larger imaging field of view.

Most of the previous works on optimizing optical forces have focused on improving the trapping beam [14–17] while structure-related force optimization mostly involves material selection and antireflection coatings [18,19] or optically driven motors based on birefringence or light scattering [20–23]. In this work we bring focus to the object shaping aspects of optimizing the mechanical effects of optical fields. We demonstrated in a recent work the optical manipulation of 2PP-fabricated free-floating waveguides [12]. Here we again consider three-dimensional waveguide structures, but now shift our attention to the force exerted by light on the waveguide and use such light-guiding to exemplify designed light deflections in structure-based force optimization. We present numerical results to estimate achievable forces when using unfocussed light to manipulate shaped microstructures. We also show proof-of-principle optical manipulation experiments of such shaped microstructures by using the free-floating waveguides originally fabricated for [12]. Finally, we present our conclusions and perspectives for using three-dimensional fabrication technologies for shaping structures to predictably divert light's momentum and achieve desired mechanical effects from optical forces. But first, we briefly review some concepts for describing the efficiency of momentum exchange in the optical trapping and manipulation in the next section.

2. Optimizing the optical force: from partial internal reflection to total internal reflections and guided waves

Ashkin originally motivated his pioneering work with the realization that optical forces can effect substantial acceleration on microscopic objects. Incident illumination can transfer as much as twice its initial momentum on a perfectly reflecting surface. The optical force exerted by incident illumination on a structure may be written as [24]:

$$F = Q\frac{n_m P}{c}. \tag{1}$$

Taking $n_m P/c$ as the total momentum flux due to light having power P incident on a structure within a surrounding medium with refractive index n_m, the quality factor, Q, therefore indicates the efficiency with which light momentum is transferred to the structure (perfect plane wave reflection at normal incidence corresponds to $Q = 2$). Using a ray optics analysis that considers multiple partial internal reflections in a dielectric microsphere [24], Ashkin estimated that $-0.276 < Q < 0.490$ as the sphere is axially translated along its equilibrium point (for $NA = 1.25$, no apodisation). The quality factor falls down to $-0.019 < Q < 0.147$ when the numerical aperture is lowered to NA ~0.64 (Gaussian apodisation). The reported experimental values of trapping efficiencies are typically lower (e.g., $Q = 0.026$ ~0.18 for $R = 5$ μm at $NA = 1.3$ [17]). The range of trapping efficiencies can vary by an order of magnitude

#176697 - $15.00 USD Received 21 Sep 2012; revised 22 Nov 2012; accepted 23 Nov 2012; published 7 Jan 2013

in the presence of aberrations when trapping through a thick sample chamber, which can somehow be recovered by aberration correction [25]. Having higher quality factors is needed to fully exploit light's momentum either to achieve stronger optical forces or to avoid the use of high input powers.

One way to interpret the poor *Q* achieved when trapping dielectric microspheres is that, in contrast to perfect reflection, the partial refractions and reflections at the material interfaces is a less efficient way of transferring momentum. For example, light reflection on silver microbeads at *NA* = 1.25 can produce axial forces with efficiencies up to *Q* ~3.5. Reflections off metallic beads are, however, complicated by heating effects and radiometric forces [26]. For dielectrics, a way to enhance Fresnel reflections is to use materials having higher refractive indices, which consequently leads to stronger optical forces. Simulations reported in [27] show that changing the refractive index from $n = 1.6$ to $n = 3.2$ increases the efficiency factor, *Q*, by one order of magnitude, which can eventually lead to transversely unstable traps for microspheres having even higher refractive indices. Similarly, the enhanced partial reflections off high-refractive index materials can also degrade the axial trapping stability, but this can be alleviated by anti-reflection (AR) coatings, which have been proposed and demonstrated [18]. Minimizing the external reflections (i.e., at low-to-high index interfaces) with AR coatings not only helps maintain stability but also leads to enhanced force when using high-index materials, which can enable breaking into the nanonewton regime, as was shown recently [19].

In our approach, we seek to enhance light reflection, without resorting to very high refractive indices, by exploiting total internal reflection. The approach relies on three-dimensional microfabrication techniques (e.g., two-photon polymerization, 2PP) to create structures for guiding light along desired paths. Having control over the light path enables the control and engineering of the optical momentum exchange. This can be used not only for enhancing optical force and torques but also for exploring other dynamical effects such as new optical manipulation modalities.

In general, there can be numerous structures for light routing, which can be designed using a variety of optimization strategies. As a start, we will only consider a simple bent waveguide here to illustrate some basic features and possibilities when using designed microstructures for tweaking optical manipulation. We have recently analyzed and demonstrated a bent waveguide that can be mechanically guided by optical traps for routing optical radiation to localized targets. This time we will focus our attention on the optical force that arises when the waveguide redirects incident light.

For quantitative analysis, we can calculate the time-averaged optical force on a bent waveguide by integrating the time-averaged Maxwell's stress tensor over a closed surface surrounding the waveguide [28]:

$$\mathbf{F} = \int_{\mathbf{S}} \left\langle \tilde{\mathbf{T}}(\mathbf{r},t) \right\rangle \cdot d\mathbf{S}, \tag{2}$$

where differential area element d**S** is directed along the outward normal and $\tilde{\mathbf{T}}$ is the Maxwell stress tensor given by

$$\tilde{T}_{ij}(\mathbf{r},t) = \varepsilon\varepsilon_0 E_i(\mathbf{r},t) E_j(\mathbf{r},t) + \mu\mu_0 H_i(\mathbf{r},t) H_j(\mathbf{r},t) - \frac{1}{2}\left[\varepsilon\varepsilon_0 \left|E(\mathbf{r},t)\right|^2 + \mu\mu_0 \left|H(\mathbf{r},t)\right|^2 \right] \delta_{ij}. \tag{3}$$

This requires finding the spatial distribution of the electric and magnetic fields, which we determined through finite-difference time domain (FDTD) simulations [29]. For computational convenience, we perform 2D simulations, where the structure and fields are assumed to be invariant along the *y* direction (the incident beam propagation is towards the + *z*-axis). As will be described below, this simplified simulation does not lose its generality and captures the main features of our proof-of-principle experiments. The FDTD simulations were performed on a 512 × 512 grid. One micrometer is scaled to 25 grid points. The incident

#176697 - $15.00 USD Received 21 Sep 2012; revised 22 Nov 2012; accepted 23 Nov 2012; published 7 Jan 2013

beam (vacuum wavelength λ_0 = 1070 nm) exhibits a Gaussian transverse profile (beam waist w_0 = 2.0 μm) along the *x*-axis and propagates through water (n = 1.33) towards the + *z*-axis with linear polarization along the *y*-axis (which can subsequently create TE–polarized modes in the waveguide). In this case, only E_y, H_x, and H_z are nonzero and Eq. (3) becomes:

$$T_{xx} = -\varepsilon\varepsilon_0 \frac{1}{2} E_y^{\,2} + \mu\mu_0 \frac{1}{2}\left(H_x^{\,2} - H_z^{\,2}\right) \tag{4a}$$

$$T_{zz} = -\varepsilon\varepsilon_0 \frac{1}{2} E_y^{\,2} + \mu\mu_0 \frac{1}{2}\left(H_z^{\,2} - H_x^{\,2}\right) \tag{4b}$$

$$T_{xz} = T_{zx} = \mu\mu_0 H_x H_z \tag{4c}$$

Calculating the optical force on a waveguide with a 2D simulation cannot give us an efficiency factor, Q_{WG}, which can be directly compared with literature values. To have a meaningful comparison, we therefore performed similar 2D simulations using a circular dielectric microbead (n = 1.6 matching SU8) as a reference object, whose diameter (d_{ref} = 1 μm) matches the input diameter of the waveguide to intercept an equal portion of the incident light. This enables us to calculate a relative efficiency factor for the optical force acting on the waveguide, $Q_{rel} = Q_{WG}/Q_{ref}$, which is simply the ratio of the optical forces, $Q_{rel} = F_{WG}/|F_{ref}|$, since we are using the same incident beam parameters for the waveguide and the reference object. Thus, the relative value obtained gives an indication of how much the efficiency factor improves compared to the circular dielectric microbead.

The simulation results for the reference bead are presented in Fig. 1, which shows the time-averaged intensity pattern and a snapshot of the transverse electric field component. For force calculations, the stress tensor is evaluated according to Eq. (2) by integrating along the bounding box shown in Fig. 1(a). The reference force obtained is practically a downward force $|F_{\text{ref}}|$ = 3.96. This force, quoted without units, is understood to be taken on an arbitrary scale, which is used consistently throughout the simulations. This arbitrary unit cancels out when calculating the relative efficiency factor, which is our quantity of interest. We also obtained comparable force results when using an alternative approach: first calculating the force on each unit cell of the simulation grid, and then summing these forces within a defined mask that is closer to the object boundary. The quiver plot overlay shows forces evaluated within 15 × 15 grid units.

The simulation results for the case of light coupling through a bent, step-index dielectric waveguide (n = 1.6 matching SU8, input diameter 1 μm) are shown in Fig. 2. Figures 2(a), 2(c), and 2(d) show snapshots of the electric and magnetic field components, while Fig. 2(b) shows the time-averaged intensity of the light propagation after 1200 time steps. Evaluating the force using the stress tensor along the box illustrated in Fig. 2(b) yields a net force, $\boldsymbol{F} = -36.14\hat{\mathbf{x}} + 37.87\hat{\mathbf{z}}$ for the TE-polarized case presented here (we obtained similar results from TM-polarized simulations). Referring back to the bead result, we get a relative efficiency factors $Q_{\text{rel,X}}$ = 9.12 and $Q_{\text{rel,Z}}$ = 9.56 along the transverse and longitudinal directions, respectively, where the axial and transverse directions are described with respect to the incident illumination. Using the net force, we get a net efficiency factor $Q_{\text{rel,net}}$ = 13.21, which represents an order-of-magnitude efficiency improvement when compared to the circular dielectric microbead.

#176697 - $15.00 USD Received 21 Sep 2012; revised 22 Nov 2012; accepted 23 Nov 2012; published 7 Jan 2013

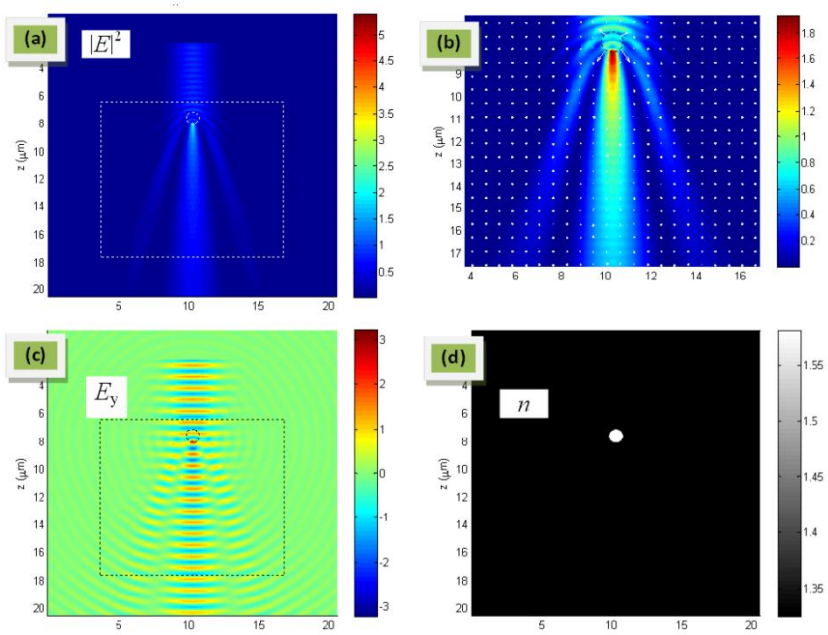

Fig. 1. Simulated scattering off a circular dielectric microbead for calculating the Maxwell stress tensor and the optical force: (a) time-averaged intensity, $|E|^2$; (b) zoom-in on the bounding box with quiver plot overlay depicting the calculated force sampled from 15 × 15 unit cells (c) snapshot of the E-field's *y*-component, E_y ; (d) refractive index distribution. (λ_0 = 1070 nm, n_{bead} = 1.6, $n_{surrounding}$ = 1.33)

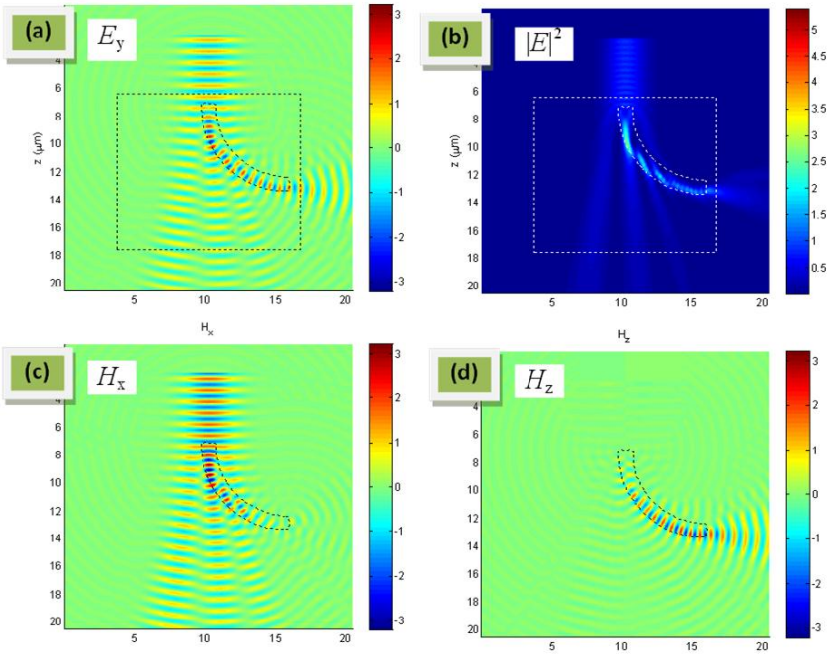

Fig. 2. Simulated propagation of light through a bent waveguide for calculating the Maxwell stress tensor and the optical force: (a) snapshot of the E-field's *y*-component, E_y; (b) time-averaged intensity, $|E|^2$; (c) snapshot of the *H*-field's *x*-component, H_y; (d) snapshot of the *H*-field's *z*-component, H_z. (λ_0 = 1070 nm, n_{bead} = 1.6, $n_{surrounding}$ = 1.33).

#176697 - $15.00 USD Received 21 Sep 2012; revised 22 Nov 2012; accepted 23 Nov 2012; published 7 Jan 2013

The results above serves as a simple example of controlled light deflection using a designed structure achieves an optical force exceeding that achieved when using simple partial reflective/refractive light deflection in a microsphere. To gauge how much more we can get with a more optimized structure for orthogonal light deflection, we also simulated the optical force that acts on a perfectly reflecting mirror angled at 45° to deflect light orthogonally. The simulation results, presented in Fig. 3, yield a net force, $\boldsymbol{F} = -86.98\hat{\mathbf{x}} + 85.62\hat{\mathbf{z}}$. The corresponding transverse, axial, and net relative efficiency factors are $Q_{\mathrm{rel},x}$ = 21.95, $Q_{\mathrm{rel},Z}$ = 21.61, $Q_{\mathrm{rel},net}$ = 30.8, respectively. The same order of magnitude efficiency improvement, relative to a circular microbead, achieved for both the waveguide and the perfect mirror indicates that, indeed, the waveguide serves as a good example of optimizing the optical force using structures designed with specifications for light deflections. Moreover, the about twice higher efficiency achieved for the perfect mirror shows that there is still some room for optimizing the deflecting structure (e.g., minimizing the coupling losses evident in the simulated propagation in Fig. 2).

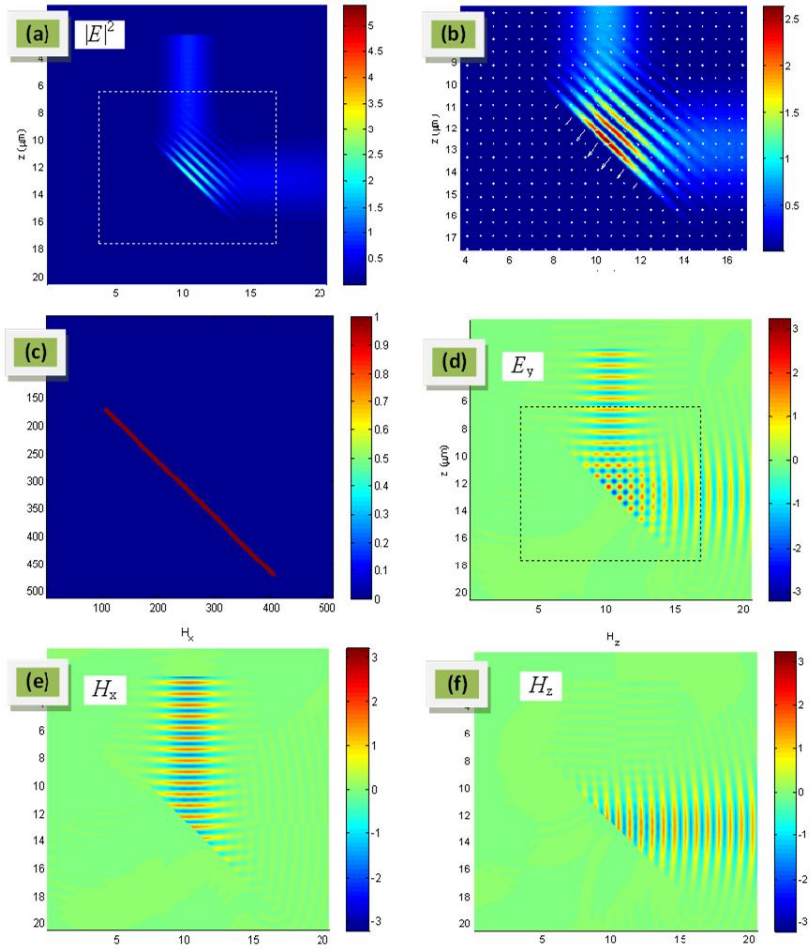

Fig. 3. Simulated reflection off a perfect mirror for calculating the Maxwell stress tensor and the optical force. (a) time-averaged intensity, $|E|^2$; (b) zoom-in on the bounding box with quiver plot overlay depicting the calculated force on each 15 × 15 grid unit of the simulation (c) location of mirror (λ_0 = 1070 nm, $n_{\mathrm{surrounding}}$ = 1.33) (d)–(f) snapshots of the fields E_y, H_x, and H_z.

#176697 - $15.00 USD Received 21 Sep 2012; revised 22 Nov 2012; accepted 23 Nov 2012; published 7 Jan 2013

It was recently demonstrated that the optical force caused by reflection off angled micromirrors (metallic thin films deposited on the surfaces of microfabricated structures) can propel microstructures and enable laser-driven autonomous robotic microswimmers [30]. In the next section we describe our experiments using microstructures fabricated with built-in waveguides. These proof-of-principle experiments will demonstrate that guided light deflections in the waveguide generates optical forces that can mechanically drive the structures that contain these waveguides.

3. Optical force on a shaped microstructure: dragging a waveguide along light tracks

To illustrate some of the features predicted by the theoretical simulation analysis in the previous section, we fabricated bent waveguides similar to those used for proof-of-concept experiments in [12]. The bent waveguides form part of a larger structure that can settle due to gravity at the bottom of the sample chamber and keep the bent waveguide oriented with its input tip pointing upward to receive light from the microscope objective above, e.g., as shown in Fig. 4(a). The fabrication procedure and parameters are described in [12] and the two-photon microfabrication system is described in [31]. In summary, the procedure includes a two-minute soft bake of spin-coated photoresist layer (SU8 2007, Microchem) before laser illumination and a 10-minute post bake after the illumination, both at 95°C on a hot plate. Microstructures were formed by scanning tightly focused ultrashort pulses from a Ti:sapphire laser (λ = 796 nm, 100 fs pulses, 80 MHz repetition rate, 3 mW average power) in the photoresist. The laser pulses were focused by an oil-immersion microscope objective (100 × Zeiss Achroplan, 1.25NA objective; DF-type immersion oil Cargille Laboratories, formula code 1261, n = 1.515). The focal spot was scanned relative to the resin at speeds of 10 μm/s for the spheres and 5 μm/s for the connecting rods and tip to solidify voxels with minimum transverse and axial feature sizes of 0.4 ± 0.1 μm in transverse and 1 ± 0.1 μm in longitudinal directions, respectively.

For optical manipulation experiments, the microstructures were injected into a cytometry cell (Hellma 131.050, 250μm × 250μm inner cross-section, 1.6 μL volume), which was then sealed and loaded in our BioPhotonics Workstation (BWS) [32]. A user operates the BWS through a LabVIEW program that handles the interface to the imaging, optical trapping and electronic hardware. The BWS software controls a beam modulation module (BMM) to create multiple beamlets from an expanded NIR light source (λ_0 = 1070 nm), which are typically used as multiple counterpropagating beam traps at the sample cell through opposite microscope objectives (Olympus LMPLN 50 × IR, WD = 6.0 mm, NA = 0.55). The point-to-point optical mapping from the beam modulation plane to the projection plane in the sample works such that the power in each beamlet scales linearly with the beamlet cross-sectional area. The beamlets can also be combined to create other patterns such as line traps. Moreover, although the BWS typically uses counterpropagating beams for optical trapping, most of the experiments described below involved microstructures resting on the chamber floor and predominantly used the downward beams only. Unless stated otherwise, only a much weaker counterpropagating upward beam was used to help visualize the downward beam when recording experiments with the topview camera. With the prior calibration and alignment, the upward beam imaged by the topview camera correctly locates the relevant downward beam.

As predicted in the previous section, guiding light through the bent waveguide exerts optical force on the waveguide having axial and transverse components. When the structure rests at the bottom of the sample chamber, the axial component of the optical force points downward and is cancelled by the normal force from the chamber floor. The transverse optical force component would then drag the structure horizontally along the chamber floor, subject to the chamber friction and fluid drag. Coupling a single static beamlet through the waveguide generates force that will displace the waveguide. This displacement will create suboptimal light coupling and, thus, the waveguide will eventually stop moving. By using a linetrap, instead of a single beamlet, we can ensure that the waveguide's input tip remains

#176697 - $15.00 USD Received 21 Sep 2012; revised 22 Nov 2012; accepted 23 Nov 2012; published 7 Jan 2013

illuminated by the same intensity even when the structure moves due to the optical force, without having to create a dynamic trap that would "chase" the waveguide around. In the present experiments, we use the BWS to create linetraps by combining beamlets. The resulting linetrap has the same intensity as an isolated beamlet and the linetrap width matches the diameter of a beamlet that is used to trap the structure at its spherical handles. For initial tests, we used a waveguide with two bends such that both ends face upwards when the structure rests on the chamber floor, as illustrated in Fig. 4(a). For a lossless waveguide, all light entering through one tip emerges out of the other. In the present case, however, bending losses allow light to escape horizontally along the bend, as confirmed by sideview microscopy image shown in Fig. 4(a). As shown in Fig. 4(b), even this partial vertical-to-horizontal light deflection along the waveguide creates sufficient horizontal force component that can exceed the combined maximum transverse force from two trapped spherical handles, which allows the structure to escape when a line trap illuminates the input tip. The experiment was done with the structure resting on the floor of the sample chamber.

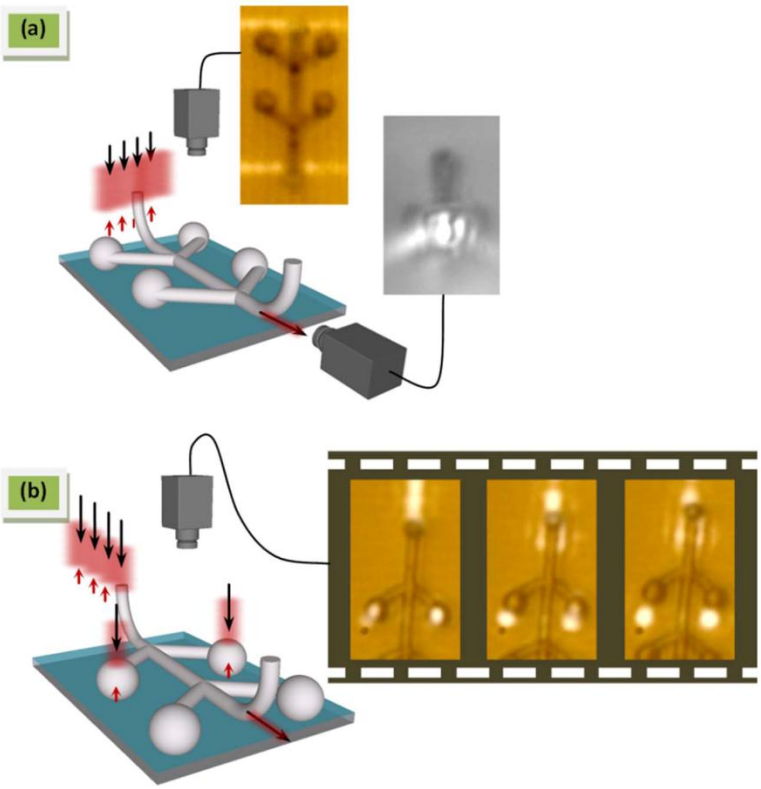

Fig. 4. Optical force on a structure though guided light deflections in its built-in waveguide. (a) Concurrent top- and side-view microscopy shows that a portion of the incident downward light entering the waveguide escapes horizontally. The light pattern seen by the top-view microscope is from the weak counterpropagating light that was calibrated and aligned to easily visualize the downward light in the microscope. (b) Optical tug-of-war: waveguide force vs. combined force from two trapped spheres. The incident light deflected by the waveguide creates downward and horizontal force components (c.f. Fig. 2). Snapshots from the top-view microscope show that the horizontal force on the waveguide can exceed the combined maximum forces on two trapped spherical handles allowing the structure to escape the traps. The line illumination and the trapping beams have the same intensity. Line illumination was used to ensure that the waveguide input is constantly illuminated even when it moves due to the waveguide force.

#176697 - $15.00 USD Received 21 Sep 2012; revised 22 Nov 2012; accepted 23 Nov 2012; published 7 Jan 2013

Figure 5 shows snapshots from video recordings of optical manipulation experiments studying the structure's motion due to the optical force on its waveguide (experimental geometry schematically depicted in Figs. 5(a') and (b')). The results presented in Figs. 5(a) and 5(b) show that the line trap effectively defines a "light track" where the microstructure glides along while it is simultaneously pushed downward against the bottom of the sample chamber. The sequential arrangement of equally time-spaced snapshots enables us to plot the structure's position vs. time by using the structure's tip as data points for the plot. The structure's position vs. time plot in Fig. 5(a) shows that it moves with fairly constant velocity until the other tip reaches the light track and gets illuminated. The constant velocity suggests that the optical force is matched by dissipative forces (in this case due to fluid drag and friction with the bottom surface of the sample chamber).

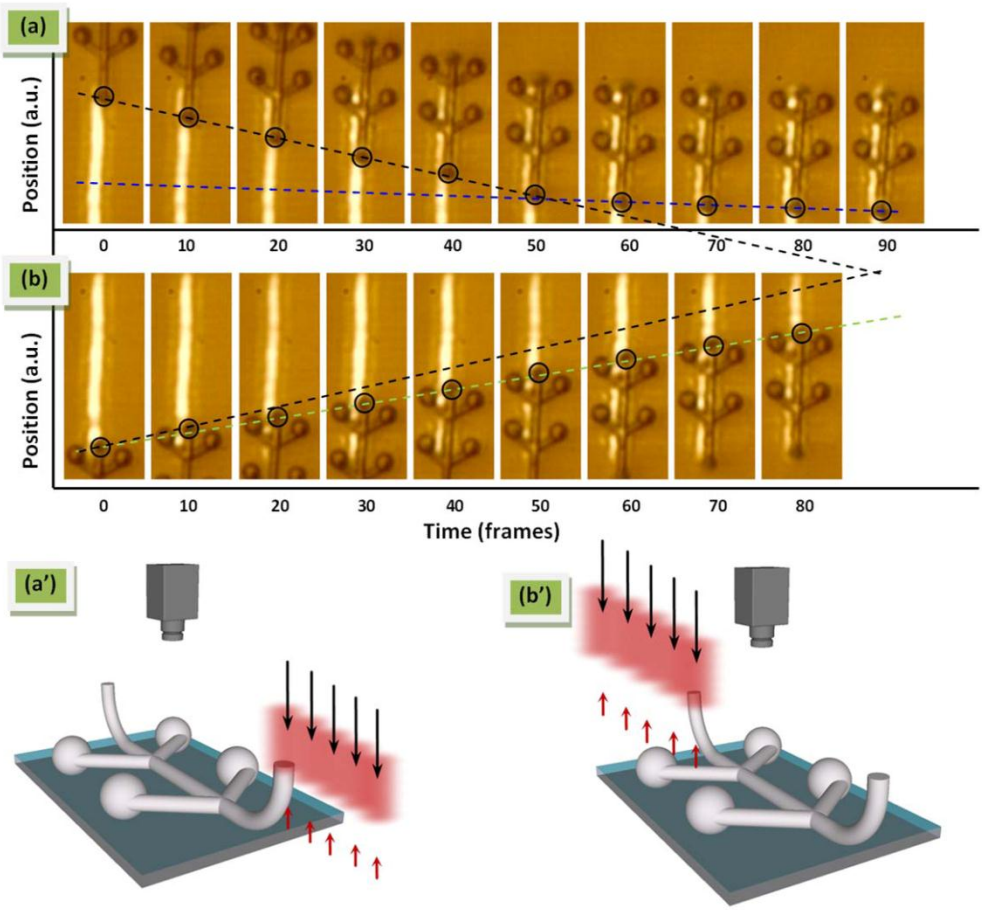

Fig. 5. Motion of a structure due to the optical force from guided light deflection. The horizontal arrangement of the snapshots, taken at equal time intervals using the top-view microscope, enables using the structure's tip as the position data point at each observation time. (a) Plot of the structure's position vs. time with light first entering one tip as shown in (a'). The trendlines indicate that the structure moves with nearly constant velocity when light enters only one tip of the waveguide (frames 0 to 50). The movement pulls the other tip into the linear illumination region; the structure subsequently moves with lower velocity when light enters both tips (frames 60 to 90); (b) Plot of the structure's position vs. time with light first entering the other tip as shown in (b'). The green trendline indicates that, with light being guided in the opposite direction, the structure also moves with a nearly constant velocity. The lower slope of the green line compared to the black line indicates that it moves slower compared to (a).

#176697 - $15.00 USD Received 21 Sep 2012; revised 22 Nov 2012; accepted 23 Nov 2012; published 7 Jan 2013

When both tips are illuminated by the linetrap (frames 50-90 in Fig. 5(a)), light is simultaneously guided in opposite directions along the waveguide, resulting in a superposition of forces due to each guiding direction. The motion plot shows that the structure continues moving, albeit with much lower velocity. This suggests that guiding light in opposite directions generate unequal forces. To verify this, we guided light in the opposite direction to that in Fig. 5(a) by illuminating only the other tip first. The resulting motion is depicted by the position vs. time plot in Fig. 5(b), which uses sequentially arranged snapshots taken at equal time intervals as basis for data points. The slope of the best-fit line indicates that the structure moves with lower speed compared to Fig. 5(a) (for comparison, a black line having the negative slope as the best-fit line in Fig. 5(a) is overlaid on Fig. 5(b)). This slower motion indicates that the guiding efficiency is different in each direction, which leads to slightly unequal forces such that the structure continues to move even when both tips are illuminated by the linetrap and light is guided in opposite directions. A microscope examination of the structure shows that the two bends have different radii. This contributes to different losses at the bends, which results in different momentum change for light guided in opposite directions.

Assuming that the dissipative force is constant, the results suggest that the optical force is position-independent for this light and structure geometry. Therefore, unlike the position-dependent, spring-like restoring force in conventional optical tweezers that requires dynamic traps to exert a constant force on moving particles, the current combination of structural and beam shaping for engineered momentum exchange enables constant optical force magnitude using only static traps, much like the motion of beads along intensity patterns with phase gradients such as programmed line traps [14] or around optical vortices. Here we are able to achieve this dynamics without applying phase programming of the illuminating beam but, instead, by exploiting the effects of guided light deflection using the fabricated structure.

The superposition of forces from multiple waveguides built into the structure can be exploited to increase the net optical force, instead of decreasing, as was the case in Fig. 5. To illustrate this, we again performed experiments to exploit waveguide effects using linetrap illumination, but using a waveguides in a different structure, as shown in the schematic diagram of Fig. 6(a). This time the structure is oriented with its spherical handles lying on a vertical plane. In this orientation, the structure is now effectively standing with its two spherical handles resting on the chamber floor and, thus, the power of the counterpropagating upward beam was increased at little to help stabilize the structure (the upward beam thus appears saturated in the top view image).

The structure's position vs. time is plotted in Fig. 6(a), again using sequentially arranged snapshots, taken at equal time intervals, and this time using a spherical handle to plot the position at various times The plot shows that the structure starts off with nearly constant speed, but shifts to a faster constant speed when the line trap illuminates near the second set of spherical handles. So, does this mean that light couples into the spherical handle, through the supporting arm, and then to the long central axis, which is then reinforced with the second set of handles is illuminated? However, analyzing the change in the optical momentum in this scenario predicts force and motion opposite to that observed here. Upon experimental verification described below, we determined that, in this case, the relevant waveguiding geometry is as depicted in Fig. 6(b). In the geometry shown in Fig. 6(b), light couples in through the central portion of the structure and, upon being guided through the supporting arms, it then effectively uses the usual spherical trapping handles as built-in microlenses for coupling light out of the structure. By symmetry, we can expect a similar guided deflection for beams that illuminate the structure from above, which will create a horizontal force component along the same direction

To verify this alternate geometry for coupling light through the microfabricated structure, we performed experiments where the microstructure is trapped within a fluorescent medium. This helps to visualize the path of another laser beam (λ = 532 nm), which is introduced from

#176697 - $15.00 USD Received 21 Sep 2012; revised 22 Nov 2012; accepted 23 Nov 2012; published 7 Jan 2013

below and viewed by the sideview microscope. This time the BWS is used in its conventional trapping mode (i.e., using balanced counterpropagating beams, λ = 1070 nm) to trap the microstructure at the spherical handles and position it relative to the static beam and illuminate different sites on the structure. The images obtained by the sideview microscope, presented in Fig. 6(c), confirms the geometry depicted in Fig. 6(b), where light couples in through the central portions of the structure where the supporting arms connect and then exit through the spherical trapping handles. Moreover, Fig. 6(c) also illustrates that the spherical trapping handles can effectively work as microlenses that serve to minimize the divergence of the light coming out of the structure. In this experiment, the green beam power was minimized to visualize the beam path without appreciably disturbing the counterpropating NIR optical traps that hold the structure through its four spherical handles. As we anticipated, illuminating the spherical handles with green light did not lead to waveguiding (a time-reversal argument based on observed beam path in Fig. 6(c) requires obliquely illuminating the spherical handle to guide light through the supporting arm).

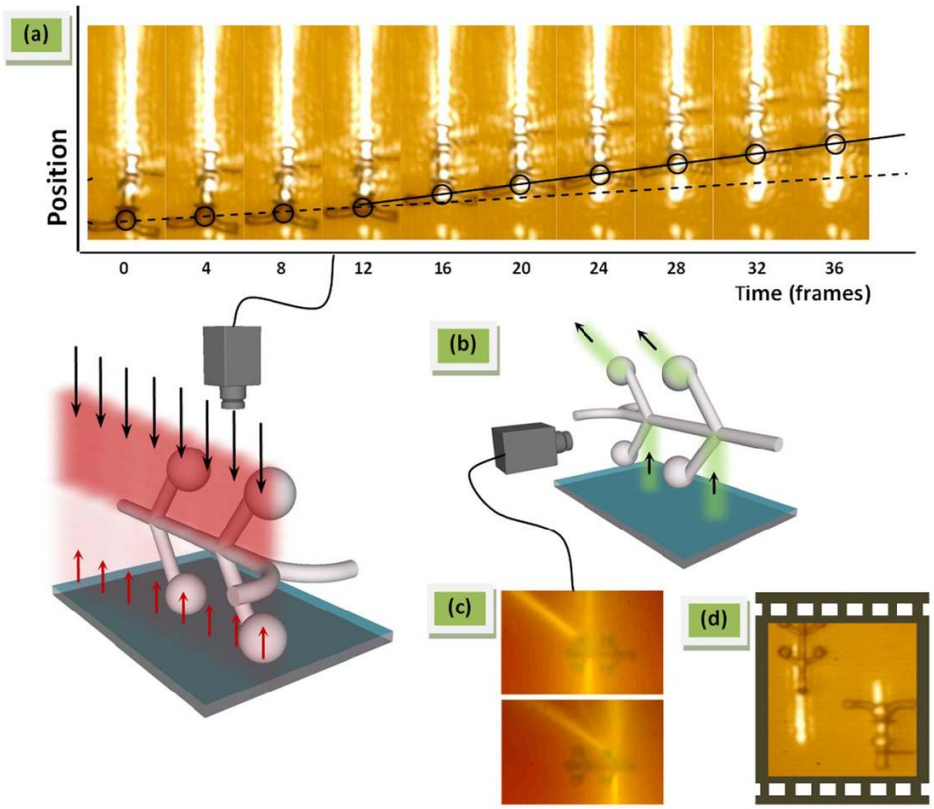

Fig. 6. Motion of structure due to the superposition of optical forces from guided light deflections. The horizontal arrangement of the snapshots, taken at equal time intervals using the top-view microscope, enables using the structure's spherical handle as the position data point at each observation time. (a) Plot of the structure's position vs. time shows two speeds– the structure increases its speed when a second guided deflection occurs and forces from the guided deflections reinforce each other. (b) Illustration of light deflection geometry having two guided light deflections whose generated forces can reinforce each other. (c) Snapshots from the sideview microscope experimentally illustrating the guided light deflection geometry illustrated schematically in (b). The experiment is performed in a fluorescent medium to help visualize the deflections of a green beam (λ = 532 nm). The structure is trapped at its spherical handles by counterpropagating infrared beams (λ = 1070 nm) to position it relative to the green beam and illuminate points that create guided light deflections; (d) (Media 1) Snapshot from the topview microscope when using two linear illumination patterns for the simultaneous optical manipulation of the two different structures used in Figs. 5 and 6(a) using line traps.

#176697 - $15.00 USD Received 21 Sep 2012; revised 22 Nov 2012; accepted 23 Nov 2012; published 7 Jan 2013

Having verified how beams can be guided through the structure, we can conclude that the observed motion of the structure in Fig. 6(a) confirms that different guided light deflections in the structure can generate transverse forces that reinforce each other. The structure initially moves as the line pattern illuminates the first in-coupling site. The transverse motion brings the structure's second light-coupling point into the illumination region, which causes the structure to speed up as the force from the additional guided light deflection reinforces the initial force. This proof-of-principle demonstration shows that structures can be designed such that different guided light deflections from the various inputs generate forces that reinforce each other. Finally, for completeness, we also present a sample video clip, recorded using the topview microscope as depicted in Fig. 6(a), which shows the structure being optically manipulated using a line trap (Media 1). Moreover, this clip also demonstrates the simultaneous optical manipulation of the two different structures used in Figs. 5 and 6(a). Figure 6(d) shows a snapshot from the video clip.

4. Conclusions and outlook

Using a bent waveguide as an example, we have shown some of the features and promising potential of shaping objects to create controlled light deflections and, thereby, achieve desired optical forces. Our numerical simulations show that a simple bent waveguide can have an order of magnitude improvement in the trapping quality factor when compared to a dielectric microbead that intercepts an equal cross-section of the incident beam. The achieved improvement is comparable to using a perfect mirror for orthogonal light deflection, which highlights the improved efficiency with which shaped structures are able to utilize the incident optical momentum flux. Our proof-of-principle experiments illustrate the possibility of optical manipulation using shaped structures. Moreover the results display an interesting optical manipulation modality where static illumination exerts a position-independent optical force, along one dimension, in contrast to harmonic potential regimes in conventional optical trapping. This "force clamp" (in analogy with the optical torque wrench [33], which can exert controlled torque) can open the possibility for exerting programmed optical forces without the need for sensitive position detection systems in various applications. An alternate approach for creating a force clamp by shaping the structure (not using waveguides, but using tapered structures) was recently published while this paper was in peer review [34]. Advanced designs in the future, developed with further optimization and potential combination of various structure-mediated light deflections, can create novel structures tailored towards specific applications. One area of interest is in utilizing this idea to create optomechanical microtools that are capable of exerting stronger forces. Another interesting application would be to use the structures, instead of microspheres, for calibrated mechanical perturbations of tethered biomolecules, where the extended structure can minimize illumination of the biomolecules to avoid optical damage and where the position-independent force profile can enable consistency in the applied force. Developing accurate force calibration methods for shaped microstructures will be an important allied technology. One approach is to use tools for calibrating trapped microspheres, e.g., position fluctuations due to thermal motion, but adapt them to the more complex dynamics of shaped structures [35]. On the other hand, emerging novel optical manipulation schemes can also demand novel calibration schemes.

Acknowledgment

This work was supported by the Danish Technical Scientific Research Council (FTP) and the Hungarian Scientific Research Fund (OTKA-NK-72375).

#176697 - $15.00 USD Received 21 Sep 2012; revised 22 Nov 2012; accepted 23 Nov 2012; published 7 Jan 2013